Microscopy and Microanalysis (2020), **26**, 1014–1023
doi:10.1017/S143192762002437X

Microscopy AND Microanalysis

Original Article

Combined Microscopic and Metabolomic Approach to Characterize the Skeletal Muscle Fiber of the Ts65Dn Mouse, A Model of Down Syndrome

Barbara Cisterna[1], Anatoly P. Sobolev[2], Manuela Costanzo[1], Manuela Malatesta[1]* and Carlo Zancanaro[1]

[1]Anatomy and Histology Section, Department of Neurosciences, Biomedicine and Movement Sciences, University of Verona, Strada Le Grazie 8, Verona I-37134, Italy and [2]Magnetic Resonance Laboratory "Annalaura Segre", Institute for Biological Systems, National Research Council, via Salaria km 29.300, Monterotondo, Rome I-00015, Italy

Abstract

Down syndrome (DS) is a genetically based disease caused by triplication of chromosome 21. DS is characterized by severe muscle weakness associated with motor deficits; however, understanding the DS-associated skeletal muscle condition is limited. In this study, we used a combined methodological approach involving light and electron microscopy, as well as nuclear magnetic resonance spectroscopy metabolomics, to investigate morphology and composition of the quadriceps muscles in the Ts65Dn mouse, a model of DS, to identify structural and/or functional trisomy-associated alterations. Morphometric analysis demonstrated a larger size of myofibers in trisomic versus euploid mice; however, myofibrils were thinner and contained higher amounts of mitochondria and lipid droplets. In trisomic mice, magnetic resonance spectroscopy showed a tendency to an overall increase in muscle metabolites involved in protein synthesis. These data strongly suggest that in DS, a sarcoplasmic hypertrophy associated with myofibril loss characterizes quadriceps myofibers. In addition, large-sized mitochondria suggestive of impaired fission/fusion events, as well as metabolites modifications suggestive of decreased mitochondrial function, were found in the trisomic muscle. Albeit preliminary, the results provided by this novel approach consistently indicate structural and compositional alterations of the DS skeletal muscle, which are typical of early aging.

Key words: mitochondria, myofiber size, nuclear magnetic resonance spectroscopy, quadriceps muscle, transmission electron microscopy

(Received 18 May 2020; revised 30 July 2020; accepted 8 August 2020)

Introduction

Down syndrome (DS) is a genetically based disease caused by triplication of chromosome 21 and affecting about 1 in 700 new borns (Parker et al., 2010). In addition to the numerous health conditions characterizing this syndrome, persons with DS exhibit severe muscle weakness associated with a deficit in motor coordination, balance, and postural control (Rigoldi et al., 2011; Malak et al., 2013). This significantly limits their daily life and functional work capacity (Carmeli et al., 2002*a*, 2002*b*; Cowley et al., 2010).

Understanding of the DS-associated muscle condition is limited. Research that utilizes animal model systems allows for a high level of experimental control, integrative methods and analyses, and the potential for studying causal biological mechanisms. A focus on animal models of DS that have translational relevance to humans would allow for studies of common and causal mechanisms involved in the muscular deficit of DS.

The Ts65Dn mouse is the most extensively studied murine model of DS having a partial trisomy involving a portion of the mouse chromosome 16, which is homologous to the human chromosome 21 (Davisson et al., 1993). The Ts65Dn mouse shares with the human condition a remarkable number of phenotypic traits, including structural and cognitive alterations of the brain, Alzheimer's-like brain pathology, craniofacial alterations, and congenital heart defects (Reeves et al., 1995; Richtsmeier et al., 2000; Moore, 2006; Choi et al., 2009). Similar to DS persons, the Ts65Dn mouse also presents DS-like motor dysfunctions inclusive of skeletal muscle weakness (Costa et al., 2010) as well as gross motor and muscle phenotypes (Costa et al., 1999). Deficits in grip strength and motor coordination, as well as running and swimming speeds, were also found (Costa et al., 2010). However, an intriguing lack of obvious functional deficit in the Ts65Dn skeletal muscle has been shown (Cowley et al, 2012). The limited number of morphological studies on the Ts65Dn locomotor muscles reports no difference in the proportion of myofiber types or myofiber size in the hindlimb of trisomic versus euploid animals (Cowley et al, 2012, 2017; Pawlikowski et al., 2018). From the metabolic point of view, microarray analysis identified alterations in pathways involved in glucose and fat metabolism, as well as ATP biosynthesis, indicating a possible limitation of mitochondrial function in the soleus muscle of Ts65Dn mice (Cowley et al., 2012). This was in agreement with the presence of structurally altered mitochondria in the

***Author for correspondence:** Manuela Malatesta, E-mail: manuela.malatesta@univr.it
Cite this article: Cisterna B, Sobolev AP, Costanzo M, Malatesta M, Zancanaro C (2020) Combined Microscopic and Metabolomic Approach to Characterize the Skeletal Muscle Fiber of the Ts65Dn Mouse, A Model of Down Syndrome. *Microsc Microanal* **26**, 1014–1023. doi:10.1017/S143192762002437X

quadriceps muscle fibers of the same mouse strain (Cisterna et al., 2014). Interestingly, low respiration rate and decreased ATP production and mtDNA content were reported in neural progenitor cells from adult trisomic Ts65Dn mice (Valenti et al., 2016); in addition, impaired mitochondrial homeostasis was reported in both persons with DS and animal models of DS (Mollo et al., 2020), thus suggesting a general alteration in mitochondrial bioenergetics and biogenesis in DS.

In the present study, we focused our attention on the quadriceps femoris muscle, considered the primary mover of the leg (Pratt & Lovering, 2014). The quadriceps muscle is mostly composed of fast type II fibers (about 90% in the mouse; Zancanaro et al., 2007), which are known to be mainly affected by age-related atrophy (Lexell, 1995). Previous works suggested, in fact, that DS is characterized by a multi-systemic early aging (Roth et al., 1996; Nakamura & Tanaka, 1998). We herein adopted an innovative approach combining light and electron microscopy, immunohistochemistry, and morphometry with nuclear magnetic resonance metabolomic analysis, with an aim at characterizing the skeletal muscle fiber of the quadriceps muscle in trisomic and euploid Ts65Dn mice. Results lead the way to powerful insight into the structural and functional characteristics of the trisomic skeletal muscle.

Materials and Methods

Animals

Ts65Dn [strain: B6EiC3Sn.BLia-Ts(17 < 16>)65Dn/DnJ] breeder mice were obtained from the Jackson Laboratory, ME, USA. The colony was maintained by breeding trisomic female mice to euploid B6EiC3Sn.BLiAF1/J males. Pups were weaned at 21 days of age. Tissue for genotyping was obtained from tail clips in p11 mice. Genotyping was accomplished by Mmu17 translocation breakpoint separated PCR (Reinholdt et al., 2011).

Sixteen (eight trisomic and eight euploid) male Ts65Dn mice (The Jackson Laboratory, ME, USA) aged 8 ± 3.10 months were initially used in this work. However, due to technical problems with specimen handling, and the limited availability of adult trisomic Ts65Dn mice in the colony, results are presented from four trisomic (two for morphology and two for ^{1}H NMR analysis) and eight euploid mice (four for morphology and four for ^{1}NMR analysis).

The mice, housed in groups of 3–4 by genotype, were maintained under standard conditions (24 ± 1°C ambient temperature, 60 ± 15% relative humidity, and 12 h light/dark cycle) and fed ad libitum with a standard commercial chow. The animals had only spontaneous free-moving activity in the cage. The trisomic mice presented deficits in balance and motor coordination by month 4 of age accordingly with previous studies (Costa et al., 1999).

The experimental protocol was approved by the Italian Ministry of Health (ref.: 538/2015-PR).

Tissue Processing

Ts65Dn mice were deeply anesthetized using Tribromoethanol (TBE) drug and perfused transcardially with 0.1 M phosphate buffer solution (PBS) followed by 4% paraformaldehyde in PBS. After perfusion, the vastus lateralis and rectus femoris muscle were quickly removed and samples (about 1 mm^3) therefrom were further placed for 2 h at 4°C in either a 2.5% glutaraldehyde plus 2% paraformaldehyde solution (samples intended for ultrastructure) or 4% paraformaldehyde and 0.2% glutaraldehyde in 0.1 M PBS (samples intended for immunohistochemical evaluation at fluorescence microscopy). After fixation, samples for ultrastructural morphology were rinsed with PBS, postfixed with 1% OsO_4 for 2 h at 4°C, dehydrated with acetone and embedded in Epon 812. For immunohistochemistry, samples were washed in PBS, treated with 0.5 M NH_4Cl solution in PBS for 45 min at 4°C to block free aldehyde groups, dehydrated in graded concentrations of ethanol at room temperature and embedded in LRWhite resin.

Due to the small size of the muscles, the rectus femoris and vastus lateralis from the right leg were used for ultrastructural morphology and those from the left leg were processed for immunohistochemistry. Each muscle was cut transversely at mid-length; during the embedding procedure, care was taken to allow for one muscle half to be sectioned transversely and the other one longitudinally.

Morphological and Morphometric Evaluation

For ultrastructural morphology, ultrathin (70–90 nm thick) sections of Epon-embedded muscles were stained with lead citrate for 1 min and observed in a Philips Morgagni transmission electron microscope operating at 80 kV and equipped with a Megaview III camera for digital image acquisition.

For fiber typing, 2 µm-thick cross sections of LRWhite embedded muscles were submitted to immunohistochemical procedures to distinguish fast and slow fibers (Zancanaro et al., 2007). Briefly, sections were incubated for 2 h at room temperature with a mouse monoclonal antibody recognizing the heavy chain of skeletal fast fiber myosin (clone MY-32, Sigma-Aldrich, Buchs, Switzerland) diluted 1:200 in PBS; the antigen–antibody complex was revealed with an Alexa 488 conjugated antibody against mouse IgG (Molecular Probes, Invitrogen, Milan, Italy). The sections were finally counterstained for DNA with 0.1 µg/mL Hoechst 33258. Micrographs were taken with an Olympus BX51 microscope equipped with a 100 W mercury lamp under the following conditions: 330- to 385-nm excitation filter (excf), 400-nm dichroic mirror (dm), and 420-nm barrier filter (bf), for Hoechst 33258; 450- to 480-nm excf, 500-nm dm, and 515-nm bf for Alexa 488. Images were recorded with an Olympus Camedia C-5050 digital camera. In immunolabeled samples, the percentage of fast and slow muscle fibers was calculated on a minimum of 100 myofibers per muscle (vastus lateralis and rectus femoris), with at least 650 myofibers measured per group (trisomic and euploid). On the same myofibers, the percentage of cells with central myonuclei was calculated. Micrographs were taken at an on-scope magnification of 20× and processed with the ImageJ software (NIH). The minimum Feret's diameter (the minimum distance of parallel tangents at opposing borders of the muscle fibers (Briguet et al., 2004) was measured on a minimum of 70 myofibers per muscle (vastus lateralis and rectus femoris) per animal, inclusive of fast and slow fibers. The minimum Feret's diameter is very insensitive against deviations from the "optimal" cross-sectioning profile, however, reliably detecting differences between muscles (Briguet et al., 2004).

For morphometric evaluation of ultrastructural variables (*Z* line length, number of mitochondria and lipid droplets, as well as mitochondrial area and cristae length), ultrathin sections of Epon-embedded, longitudinally sectioned muscle were used. Measurements were made by using the Radius software for image acquisition and elaboration implemented in the Philips Morgagni transmission electron microscope. In order to analyze myofibril size, the *Z* line length (an estimate of sarcomere

diameter; Luther, 2009) of at least 50 myofibrils per muscle (vastus lateralis and rectus femoris) per animal was measured (at a microscope magnification of 7,100×), avoiding the myofiber periphery. The area of intermyofibrillar mitochondria and lipid droplets was also measured (again at a microscope magnification of 7,100×); their respective total areas were calculated and expressed as the percentage of measured myofiber area (300 μm^2 per muscle and animal). Finally, the sectional area and the length of outer and inner mitochondrial membrane were measured (at a microscope magnification of 28,000×) in 20 intermyofibrillar and 20 subsarcolemmal mitochondria per muscle per animal, and the inner/outer membrane ratio was calculated as an assessment of cristae extension independent of mitochondrial size.

Nuclear Magnetic Resonance Spectroscopy

Despite its relatively low sensitivity, NMR spectroscopy is capable of identifying hundreds of molecules in a single sample and is rapid, nondestructive, highly reproducible, and amenable to quantification (Nicholson et al., 1999) and proved to be suitable for the investigation of different biological matrices (Zancanaro et al., 1994, 2001, 2002; Righetti et al., 2003; Zancanaro et al., 2007) inclusive of skeletal muscle (Sobolev et al., 2017).

Mice were killed by cervical dislocation, and the vastus lateralis and rectus femoris muscles were immediately dissected out, blotted on filter paper, weighed, and frozen in liquid nitrogen. Frozen specimens were then freeze-dried, ground to powder, and extracted in a mixture of methanol and chloroform as previously described (Zancanaro et al., 1994). The resulting aqueous and organic fractions were dried and stored at −80°C until analysis.

The dry residues of the aqueous fraction were dissolved in 0.72 mL of D_2O/phosphate buffer (100 mM, pH = 7) containing 1 mM 3-(trimethylsilyl)-propionic-2,2,3,3-d_4 acid sodium salt (TSP) as an internal standard. Dry organic fraction samples were dissolved in 0.72 mL of $CDCl_3/CD_3OD$ 2:1 v/v mixture with tetramethylsilane (TMS), 0.03% v/v. The NMR spectra of aqueous and organic fractions were recorded at 27°C on a Bruker AVANCE 600 NMR spectrometer operating at the proton frequency of 600.13 MHz. ^1H spectra were referenced to the methyl group signal of TSP ($\delta = 0.00$ ppm) in D_2O, and to the CH_3 signal of TMS in $CDCl_3/CD_3OD$, respectively. ^1H spectra of aqueous extracts were acquired using the same experimental conditions previously reported (Sobolev et al., 2017). The following parameters were employed to obtain ^1H spectra in $CDCl_3/CD_3OD$ mixture: 128 transients, 32 K data points, spectral width 7.184 kHz, recycle delay of 5 s, and a 30° pulse of 3 µs. TOPSPIN 1.3 Bruker software was used for the acquisition and spectral processing of the NMR data. After Fourier transformation, manual phase and baseline corrections were carried out. Assignment of spectra was conducted as previously described (Mannina et al., 2008; Sobolev et al., 2017).

A representative spectrum of the aqueous and organic fractions of muscle extract is presented in Figure 1 together with peak assignment for all metabolites that were quantified using NMR data. For the quantitative analysis, the integrals of relevant resonances in ^1H NMR spectra were measured (Table 1).

In the case of aqueous samples, the integral values were normalized with respect to the integral of the standard TSP (methyl group signal) set to 100 and divided by sample wet weight and used for quantitative analysis. In the case of $CDCl_3/CD_3OD$ spectra, a previously described procedure was followed (Sobolev et al., 2017) with some exceptions. All integrals were normalized with respect to the integral of α-CH_2 groups of all fatty acid chains ($I_4 + I_5/2$) set to 100%. The content (molar percentage, %mol) of fatty acids of four different types (saturated fatty acids, SFA, monounsaturated fatty acids, MUFA, diunsaturated fatty acids, DUFA, and polyunsaturated fatty acids, PUFA) was calculated according to equations (1)–(4).

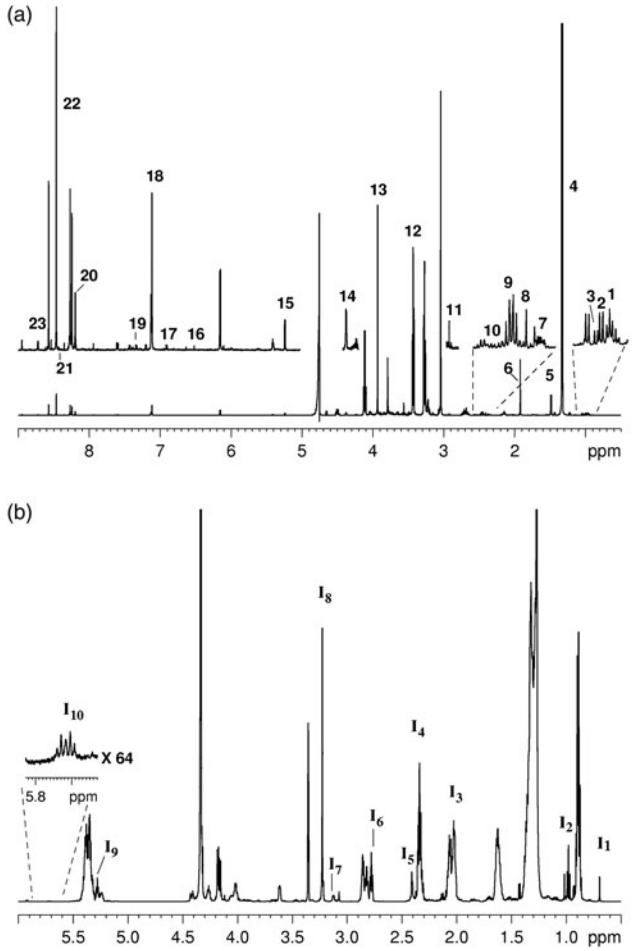

Fig. 1. ^1H 600 MHz NMR spectra of aqueous (**a**) and organic (**b**) fractions of muscle extract. Assignment of aqueous extract: 1, leucine; 2, valine; 3, isoleucine; 4, lactic acid; 5, alanine; 6, acetic acid; 7, glutamic acid; 8, succinic acid; 9, glutamine; 10, acetyl-carnitine; 11, TMA/DMA; 12, taurine; 13, creatine/ phosphocreatine; 14, inosine-monophosphate; 15, α-glucose; 16, fumaric acid; 17, tyrosine; 18, anserine/carnosine; 19, phenylalanine; 20, carnosine; 21, NAD+; 22, formic acid; 23, nicotinamide. Assignment of organic extract: I_1, Chol; I_2, PUFA; I_3, UFA; I_4, FA; I_5, DHA; I_6, DUFA; I_7, PE; I_8, PC + SMN; I_9, TG; I_{10}, SMN. See Table 1 for explanation of abbreviations.

$$SFA = 100 - I_3/2; \quad (1)$$

$$MUFA = 100 - SFA - I_6 - I_2 \times 2/3; \quad (2)$$

$$DUFA = I_6; \quad (3)$$

$$PUFA = I_2 \times 3/2; \quad (4)$$

The content of lipids (TG, PE, and SMN) was calculated using equations (5)–(7).

$$TG = I_9 \times 6; \quad (5)$$

Table 1. Assigned ^{1}H NMR Resonances of Aqueous and Organic Muscle Extracts Selected for Quantitative Analysis.

Aqueous Fraction			Organic Fraction			
Compound	Abbreviation	^{1}H (ppm)	Index	Compound (Group)	Abbreviation	^{1}H (ppm)
Acetic acid	AA	1.96	I_1	Cholesterol (CH_3)	Chol	0.70
Acetyl-carnitine	Ac-Car	2.53	I_2	Polyunstaturated fatty acids (CH_3)	PUFA	0.98
Alanine	Ala	1.49	I_3	All unsaturated fatty acids (allylic CH_2)	UFA	2.04
Anserine	ANS	7.10[a]	I_4	All fatty acids except DHA (CH_2-2)	FA	2.34
Carnosine	CAR	8.22	I_5	4,7,10,13,16,19-Docosahexaenoic acid (CH_2-2,3)	DHA	2.41
Creatine/Phosphocreatine	Cr/PCr	3.94	I_6	Diunsaturated fatty acids (CH_2-diallyl)	DUFA	2.78
Formic acid	FOA	8.45	I_7	Phosphatidylethanolamine [$(CH_3)_3N$]	PE	3.13
Fumaric acid	FA	6.52	I_8	Phosphatidylcholine + Sphyngomyelin [$(CH_3)_3N$]	PC + SMN	3.22
αGlucose	GLC	5.23	I_9	Triacylglicerols (*sn* 2-CH)	TG	5.28
Glutamine	Gln	2.46	I_{10}	Sphyngomyelin (CH)	SMN	5.72
Glutamic acid	Glu	2.35				
Inosine-monophosphate	IMP	4.38				
Isoleucine	Ile	1.02				
Lactic acid	LA	1.34				
Leucine	Leu	0.97				
NAD+	NAD+	8.43				
Nicotinamide	NCA	8.72				
Phenilalanine	Phe	7.32				
Succinic acid	SA	2.41				
Taurine	TAU	3.43				
Trimethylamine/Dimethylamine	TMA/DMA	2.92				
Tyrosine	Tyr	6.90				
Valine	Val	1.00				

The corresponding chemical shift in parts per million (ppm) is reported as well (see also Fig. 1). Index, integrals of organic fraction resonances labeled with number (I_1–I_{10}) for use in equations reported in the text.
[a]Signals of anserine and carnosine are partially overlapped, the integral from anserine was calculated as the difference between the total integral and the integral of carnosine determined using another signal (at 8.22 ppm).

$$PE = I_7 \times 2; \quad (6)$$

$$SMN = I_{10} \times 2. \quad (7)$$

PC content was calculated considering the overlapping of its characteristic signal from $N(CH_3)_3$ group with those of SMN, see equation (8).

$$PC = 4 \cdot (I_8 - I_{10} \times 9)/9. \quad (8)$$

Statistical Analysis

Data of morphometric evaluations are presented as means ± standard deviation (SD). One-way ANOVA was used for group–group comparison. For the other variables (percentage of slow fibers, percentage of myofibers with central nuclei, and ^{1}H NMR metabolites), data are presented as the median (interquartile range, IQ). Group–group comparison was performed with the Mann–Whitney test (Table 2). Statistical significance was set at $\alpha \leq 0.05$. The IBM-SPSS (v.25) statistical package was used for all analyses.

Results

Immunohistochemistry and Morphometry

Immunolabeling for the heavy chain of skeletal fast fiber myosin (Figs. 2a, 2b) revealed a similar percentage of slow fibers in trisomic and euploid animals in both the vastus lateralis muscle (median: 0.59 versus 1.09%, $p = 0.355$) and the rectus femoris muscle (median: 2.25 versus 0.00%, $p = 0.140$).

The percentage of myofibers with central nuclei increased in the rectus femoris muscle of trisomic versus euploid mice at the limit of statistical significance (median: 9.32 versus 0.62%, $p = 0.064$). The percentage of myofibers with central nuclei in the vastus lateralis muscle was similar in trisomic and euploid animals (median: 5.26 versus 7.58%, $p = 1.00$).

Minimum Feret's diameter of fast fibers was significantly higher in trisomic versus euploid mice in the rectus femoris muscle (93.36 ± 21.22 μm versus 86.86 ± 22.95 μm; $p = 0.005$) and, to an even greater extent, in the vastus lateralis muscle (100.49 ± 25.43 μm versus 89.20 ± 19.56 μm; $p < 0.001$). Figures 2c–2f show the minimum Feret's diameter distribution in fast fibers. Fast fiber size was significantly larger in the vastus lateralis muscle

Table 2. Comparison of the Amounts of Selected Metabolites in Euploid and Trisomic Quadriceps Muscle.

	Euploid ($n = 4$)	Trisomic ($n = 2$)	Z Value	Value
Metabolite (nmol/mg)				
Leucine	0.124 (0.023)	0.109	−1.389	0.165
Acetic acid	1.62 (0.61)	2.60	−1.389	0.165
Glutamate	0.158 (0.022)	0.253	−1.852	0.064
Succinic acid	0.104 (0.042)	0.168	−1.852	0.064
TMA/DMA	0.019 (0.005)	0.024	−1.852	0.064
Creatine/Phosphocreatine	12.83 (2.55)	16.57	−1.852	0.064
Metabolite (%mol)				
MUFA	40.36 (10.84)	26.94	−1.852	0.064
DUFA	22.99 (4.87)	29.16	−1.852	0.064
PUFA	4.28 (1.20)	8.55	−1.852	0.064
PE	3.34 (1.62)	7.54	−1.852	0.064

Mann–Whitney test. The median (interquartile range) is presented.
TMA/DMA, trimethylamine/dimethylamine; MUFA, monounsaturated fatty acids; DUFA, diunsaturated fatty acids; PUFA, polyunsaturated fatty acids; PE, phosphatidylethanolamine.

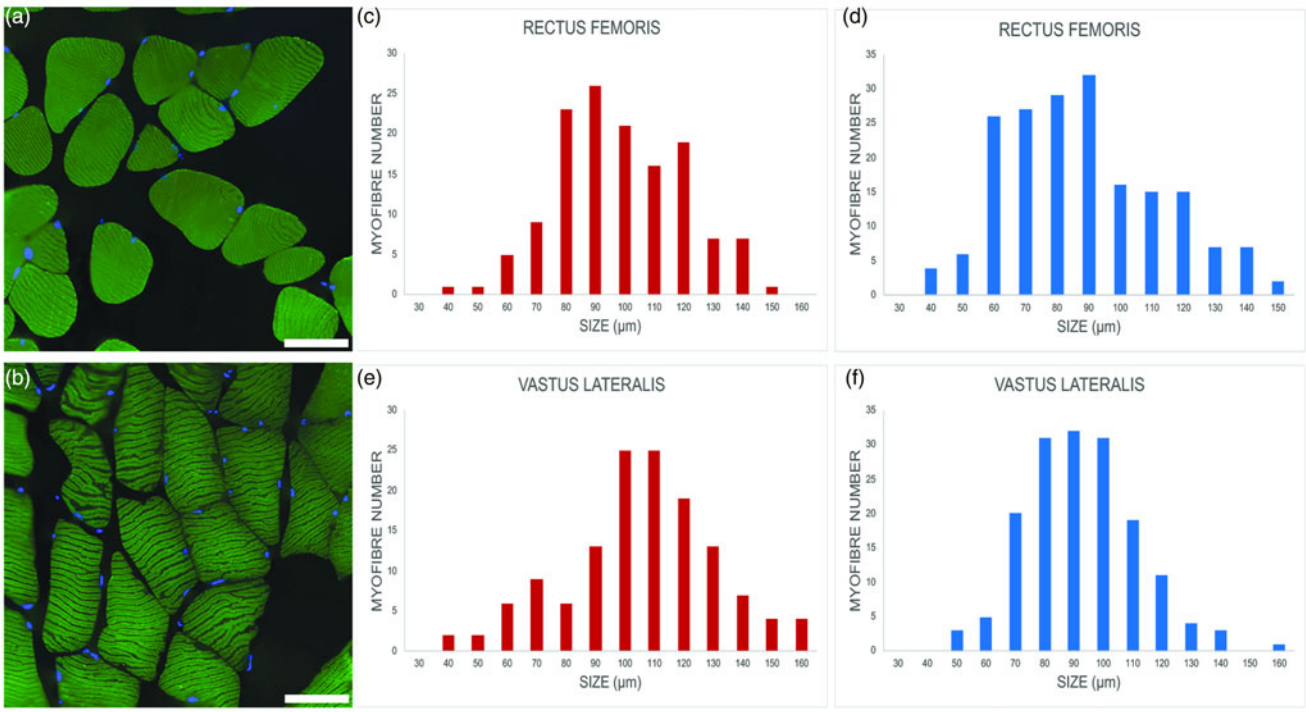

Fig. 2. Representative images of myofibers from euploid, (**a**) and trisomic, (**b**) mice; immunolabeling against the heavy chain of skeletal fast fiber myosin (green); DNA counterstaining with Hoechst 33258 (blue). Bars, 100 μm. (**c–f**) Minimum Feret's diameter distribution of the fast myofibers in the vastus lateralis and rectus femoris of trisomic (**c,e**) and euploid (**d,f**) mice. The myofibers are grouped in size classes of 10 μm and the number of fibers in each class is plotted.

versus rectus femoris muscle in trisomic ($p = 0.013$) but not in euploid ($p = 0.18$) mice. Due to the very limited number of slow fibers, no statistical analysis was carried out.

Ultrastructure and Morphometry

Morphological evaluation at transmission electron microscopy revealed that, in both euploid and trisomic mice, myofibers of rectus femoris and vastus lateralis muscles showed their typical elongated shape: the cytoplasm was almost entirely occupied by longitudinally arrayed myofibrils, while ovoid mitochondria were lined in narrow sarcoplasm areas between myofibrils and many nuclei containing a few heterochromatin clumps occurred in subsarcolemmal position. However, some fine structural differences were found between euploid and trisomic mice in both the vastus lateralis (Fig. 3) and rectus femoris (Fig. 4) muscles. In particular, in trisomic mice, both muscles showed myofibers containing irregularly arrayed myofibrils characterized by heterogeneous size and pattern, although the sarcomeric organization was preserved (Figs. 3b, 4a). In addition, large-sized mitochondria rich

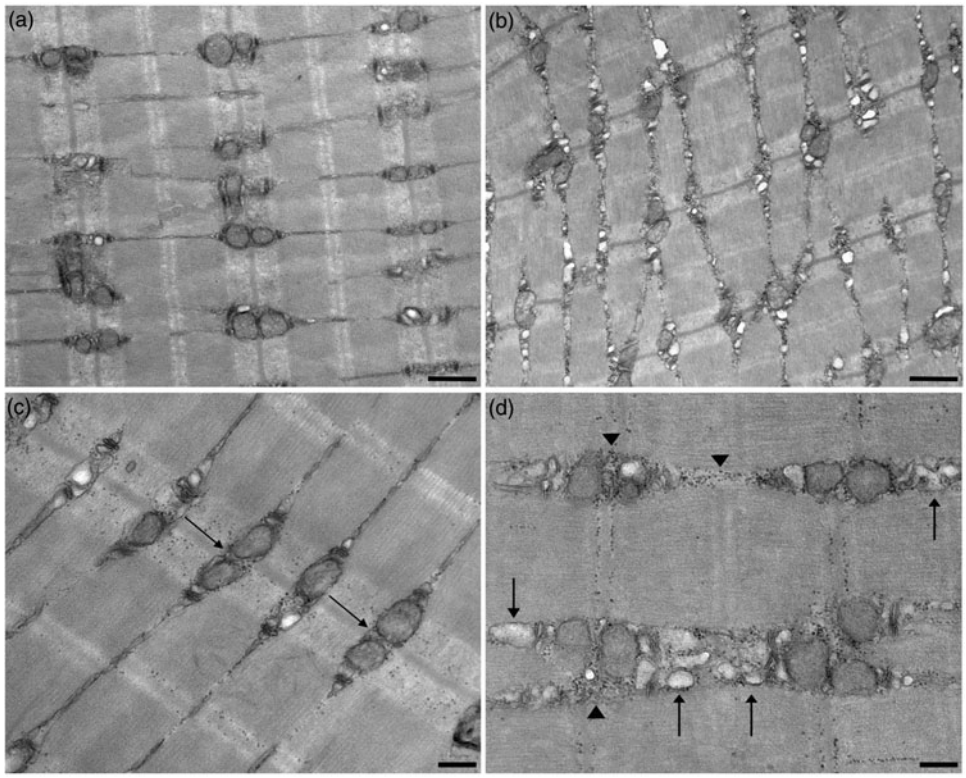

Fig. 3. Transmission electron micrographs of vastus lateralis myofibers from euploid (**a,c**) and trisomic (**b,d**) mice. (**a,c**) The cytoplasm is occupied by regularly arrayed myofibrils with well-preserved triad areas (arrows). (**b,d**) Irregularly arrayed myofibrils characterise the myofiber. Note the dilated sarcoplasmic reticulum (arrows) and the glycogen deposits (arrowheads). Bars: 500 nm (**a,b**); 200 nm (**c,d**).

in cristae were lined between the myofibrils (Figs. 3b, 3d, 4a, 4b), as well as in the subsarcolemmal region. In the vastus lateralis muscle of trisomic mice, the sarcoplasmic reticulum was characterized by dilated cisternae, as well as by deposits of glycogen especially around the intermyofibrillar mitochondria and sarcoplasmic reticulum (Fig. 3d), while lipid droplets were scarce. Conversely, numerous lipid droplets typically associated with mitochondria were found in the rectus femoris muscle of trisomic mice (Fig. 4b), whereas no sarcoplasmic reticulum enlargement or glycogen accumulation was observed.

Morphometric analysis demonstrated that the length of *Z* line was significantly lower in trisomic versus euploid animals in both vastus lateralis (327.78 ± 189.88 nm versus 451.59 ± 147.79 nm; $p < 0.001$) and rectus femoris (262.77 ± 150.21 nm versus 411.69 ± 147.65 nm; $p < 0.001$) muscles. The high SD for the trisomic *Z* line confirmed the high heterogeneity in myofibril size observed at TEM in these animals (see Fig. 3b). Figure 5 shows the *Z* line length distribution. The percentage of myofiber area occupied by the mitochondria was significantly higher in trisomic versus euploid mice in the vastus lateralis muscle (4.12 ± 0.64 versus $2.32 \pm 0.80\%$; $p < 0.005$) and, to an even greater extent, in the rectus femoris muscle (16.04 ± 3.47 versus $3.87 \pm 0.88\%$; $p < 0.001$). In the rectus femoris muscle, the percentage of myofiber area occupied by lipid droplets was significantly higher in trisomic versus euploid mice (0.49 ± 0.27 versus $0.01 \pm 0.02\%$; $p < 0.001$). The sectional area and the inner/outer membrane ratio of

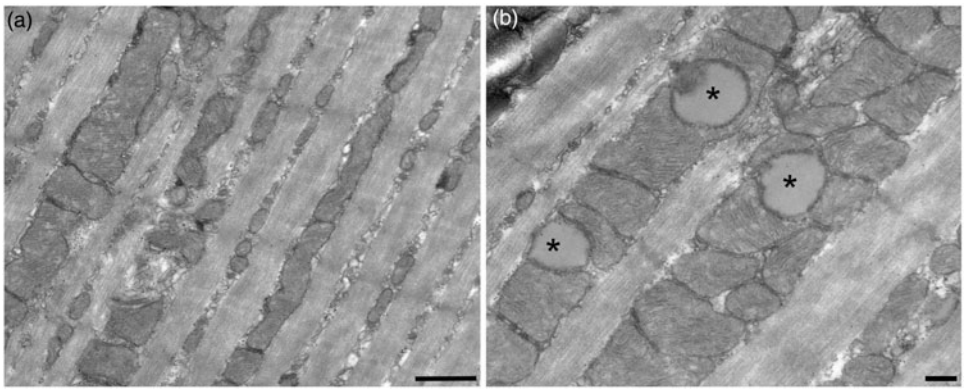

Fig. 4. Transmission electron micrographs of rectus femoris myofibers of trisomic mice. Myofibrils heterogeneous in size occur in the myofiber (**a**). Numerous lipid droplets (asterisks) are associated with large-sized mitochondria (**b**). Bars: 500 nm (**a**); 200 nm (**b**).

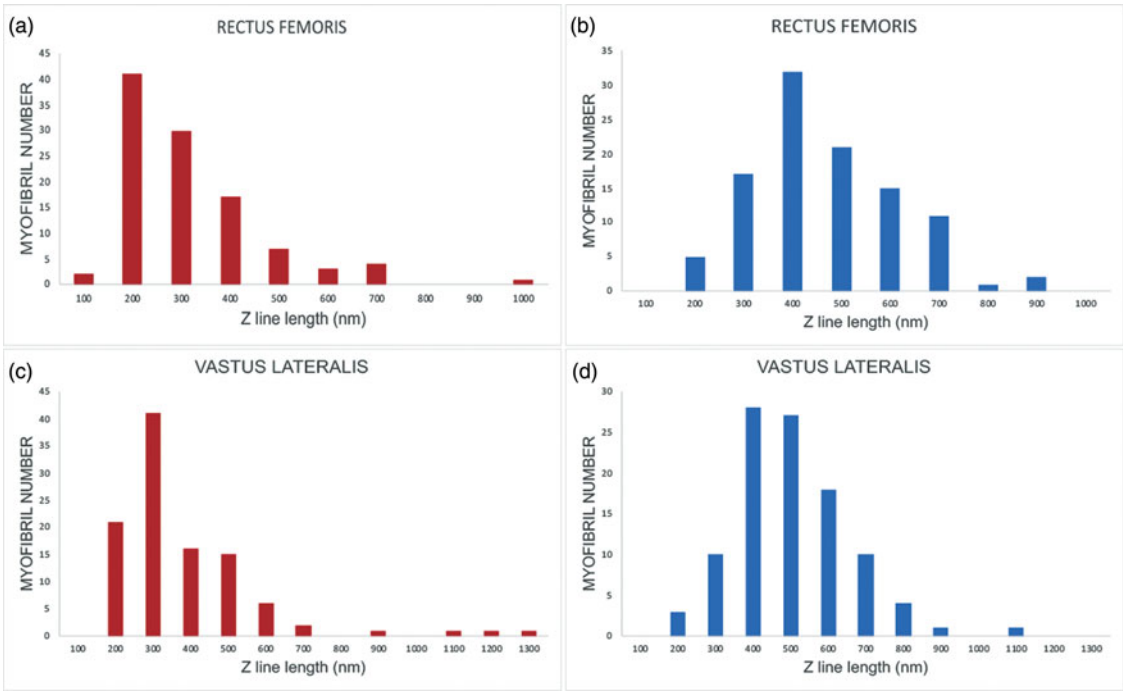

Fig. 5. Distribution of *Z* line length in the rectus femoris and vastus lateralis muscle of trisomic (**a,c**) and euploid (**b,d**) mice. The myofibrils are grouped in size classes of 100 nm and the number of myofibrils in each class is plotted.

intermyofibrillar and subsarcolemmal mitochondria were significantly higher in trisomic versus euploid mice in both rectus femoris and vastus lateralis muscles (Tables 3 and 4).

Nuclear Magnetic Resonance Spectroscopy

Several intermediate metabolism compounds (succinic acid, lactic acid, acetic acid, pyruvic acid), amino acids (e.g. leucine, isoleucine, valine, alanine, tyrosine), nucleosides (NAD+), as well as key molecules for muscle energetics (α-glucose, creatine/phosphocreatine), were identified unambiguously in the aqueous fraction and quantified (Table 1). In the organic fraction, MUFA, DUFA, PUFA, as well as cholesterol, triglycerides, and phospholipids, were identified and quantified (Table 1). Comparison of quadriceps spectra showed a tendency for some metabolites to be present in different amounts in the muscles of trisomic versus euploid mice (Table 2). In trisomic versus euploid mice, the aqueous metabolites glutamate, succinic acid, TMA/DMA, and creatine/phosphocreatine were present in higher amounts per unit wet tissue. In the organic fraction, DUFA and PUFA were present in higher amounts per unit wet tissue in the trisomic versus euploid muscle, together with phosphatidylethanolamine; instead, larger amounts of MUFAs were found in the euploid muscle. All differences were at the limit of statistical significance ($p = 0.064$).

Discussion

The Ts65Dn mouse model shares numerous phenotypes with the DS human condition among which is the DS-associated locomotory deficiency. However, it has been used to a limited extent for investigating muscle pathology in DS. In this work, we expanded on previous knowledge by exploring the structure and composition of the quadriceps muscle using a combined morphological, morphometric, and metabolomic approach. Several trisomy-associated changes were found.

A similar proportion of fast and slow fibers was found in the muscle of euploid and trisomic Ts65Dn mice (consistent with previous findings in the soleus muscle; Cowley et al., 2012); instead, myofiber size was significantly greater in trisomic versus euploid mice (rectus femoris, +7.2%; vastus lateralis, +12.6%).

Table 3. Mean ± SD Values of the Sectional Area and Inner/Outer Membrane Ratio of Intermyofibrillar Mitochondria in the Rectus Femoris and Vastus Lateralis Muscle from Euploid and Trisomic Mice.

	Mitochondrial Area (μm^2)		Inner/Outer Membrane Ratio	
Mice	Rectus Femoris	Vastus Lateralis	Rectus Femoris	Vastus Lateralis
Euploid	0.064 ± 0.028	0.050 ± 0.022	1.834 ± 0.447	1.697 ± 0.440
Trisomic	0.112 ± 0.060	0.102 ± 0.053	2.028 ± 0.504	2.124 ± 0.376
	$p < 0.001$	$p = 0.013$	$p = 0.038$	$p = 0.025$

One-way ANOVA.

Table 4. Mean ± SD Values of the Sectional Area and Inner/Outer Membrane Ratio of Subsarcolemmal Mitochondria in the Rectus Femoris and Vastus Lateralis Muscle from Euploid and Trisomic Mice.

	Mitochondrial Area (μm^2)		Inner/Outer Membrane Ratio	
Mice	Rectus Femoris	Vastus Lateralis	Rectus Femoris	Vastus Lateralis
Euploid	0.232 ± 0.113	0.194 ± 0.123	1.186 ± 0.713	1.449 ± 0.311
Trisomic	0.364 ± 0.142	0.288 ± 0.111	2.827 ± 0.790	2.047 ± 0.444
	$p < 0.001$	$p < 0.001$	$p < 0.001$	$p = 0.023$

One-way ANOVA.

This finding should be considered as preliminary due to the limited number of analyzed animals; however, it suggests the presence of trisomy-associated hypertrophy in myofibers. Accordingly, earlier work found reduced "density" of nuclei in isolated skeletal muscle fibers of persons with DS versus euploid controls (Landing & Shankle, 1982), thereby suggesting that increased myofiber size is also present in the human trisomy. Further, in the myocardium of persons with DS, cells were found to be enlarged in comparison to controls (Recalde et al., 1986). Interestingly enough, several studies showed that some proteins codified by genes located in the so-called Down Syndrome Critical Region (DSCR) are involved in the calcineurin-NFAT signaling (Rothermel et al., 2003; Arron et al., 2006; Gwack et al., 2006), which regulates a hypertrophic pathway in myofibers (Dunn et al., 1999; Semsarian et al., 1999; Ferreira et al., 2019) and cardiomyocytes (Molkentin et al., 1998). Such a pathway undergoes destabilization in DS (Arron et al., 2006). In the Ts65Dn mouse, the expression pattern of DSCR genes is similar to that in humans (Strippoli et al., 2000) and DSCR protein expression is upregulated in comparison with euploid animals (Baek et al., 2009), thus constituting a possible mechanism to explain our findings.

Skeletal muscle hypertrophy is usually characterized by an increase in myofiber protein synthesis (Bodine et al., 2001); accordingly, ^{1}H NMR showed a tendency in the trisomic mice to an overall increase in metabolites, such as glutamate and succinic acid, which are involved in skeletal muscle protein synthesis (Martins-Bach et al., 2012; Yuan et al., 2017). ^{1}H NMR also showed a tendency for phosphatidylethanolamine and polyunsaturated fatty acids to increase, and for MUFAs to decrease in muscles of trisomic mice, consistently with the activation of the mTor-pathway-independent mechanism of hypertrophy (Conte et al., 2019). In this view, the increase in the percentage of myofibers with central nuclei found in the rectus femoris of trisomic versus euploid mice, although at the limit of the statistical significance, deserves consideration. Central myonuclei are a marker of muscle regeneration/remodelling (Fukada, 2018) and satellite cells are the source of new myonuclei (van der Meer et al., 2011; Fukada, 2018). Therefore, it could be inferred that in the rectus femoris muscle, a higher regeneration/remodelling activity takes place in trisomic versus euploid mice. The lack of a corresponding finding in the vastus lateralis muscle has no obvious explanation. Since active satellite cells preferentially occur close to capillaries (Hendrickse & Degens, 2019) and the rectus femoris is characterized by more vascularized myofibers than the vastus lateralis (Johnson et al., 1973; Koga et al., 2012, 2017), a higher incorporation of satellite cells in the rectus femoris muscle may be assumed, thus contributing to muscle hypertrophy. We may therefore hypothesize that the hypertrophy of quadriceps myofibers in trisomic mice is sustained by an increase in both protein synthesis (satellite cell-independent hypertrophy, Blaauw et al., 2009) and satellite cell contribution (Fukada, 2018).

It is worth noting that, despite the increase in myofiber size in the rectus femoris and vastus lateralis muscle of trisomic mice, a reduction in *Z* line length (i.e., sarcomere diameter) occurred in both trisomic muscles in parallel to an increase in mitochondria or lipid droplets (in the rectus femoris), or sarcoplasmic reticulum and glycogen (in the vastus lateralis). Taken together, these findings suggest that the hypertrophic drive observed in the quadriceps muscle of trisomic mice leads to the so-called "sarcoplasmic hypertrophy" i.e., a myofiber growth mostly related to an increase in the volume of mitochondria and sarcoplasmic reticulum and/or sarcoplasmic enzyme or substrate content (Haun et al., 2019). The parallel, intriguing reduction in myofibril diameter found in trisomic mice could be related to an early age-related muscle wasting process since a similar reduction in myofibril size was reported in hindlimb muscles of old rats (Ansved & Edström, 1991). However, *in vivo* magnetic resonance imaging showed similar hindlimb muscles volume in trisomic and euploid Ts65Dn mice (unpublished results) suggesting that trisomy does not affect overall muscle size. These findings highlight the need for further work at the muscle organ level, taking into consideration all the histological components, in the Ts65Dn mouse model of DS.

The ultrastructural analysis and the morphometric evaluation presented herein demonstrated in the myofibers of trisomic mice the presence of large-sized mitochondria in both the vastus lateralis and the rectus femoris muscles. It is known that the balance between mitochondrial fission and fusion processes is impaired in DS (Gomez et al., 2020; Parra et al., 2018). In fact, the increase in the levels of the DSCR1 protein (also called RCAN1), affecting the calcineurin-DRP1 pathway (Gomez et al., 2020), leads to the inhibition of mitochondrial fission (Parra et al., 2018). This would be consistent with the finding of large-sized mitochondria in our trisomic mice. The presence of mitochondria with larger size and longer cristae in myofibers of the trisomic mice may not imply a higher organelle efficiency. Actually, alterations in glucose and fat metabolism and in ATP biosynthesis suggestive of mitochondrial functional limitations have been reported in skeletal muscle of Ts65Dn mice (Cowley et al., 2012). Consistently, a lower basal VO_2 (Cefalu et al., 1998) was found in these mice, and mitochondrial dysfunctions have been reported in brain tissue from DS patients (Busciglio et al., 2002).

DS is usually related to a multi-systemic early aging (Roth et al., 1996; Nakamura & Tanaka, 1998) and various alterations in mitochondrial structure and function have been found in several DS cell types (Druzhyna et al., 1998; Busciglio et al., 2002; Helguera et al., 2013; Cisterna et al., 2014). Enlarged mitochondria have been described in the aging skeletal muscle, probably as a result of impaired fission/fusion events, together with a decreased mitochondrial function (Nourshahi et al., 2012; Tassinari et al., 2019). Consistently, the increase in Cr/PCr and succinic acid highlighted by ^{1}H NMR in the present study in trisomic mice suggests perturbations in the mitochondria fuel utilization (Martins-Bach et al., 2012; Consitt et al., 2016). Accumulation of intramyocellular lipid droplets, as well as altered glycogen content, are also common features of aged skeletal muscles, likely due to the multifactorial deterioration of biological functions typical of the aging process, among which are decreased autophagic capacity, increased oxidative stress and inflammation (Shou et al., 2020). ^{1}H NMR showed a tendency for glutamate to increase and for leucine to decrease in the skeletal muscle of trisomic mice. Amino acids are known to play a regulatory role in aging (Canfield & Bradshaw, 2019) and high levels of glutamate have been described in aged skeletal muscles (Stuerenburg et al., 2006), as well as in some muscular diseases (Martins-Bach et al., 2012). Leucine is strictly related to glutamate metabolism and is involved in skeletal muscle regeneration in aging (Pereira et al., 2015) and inflammation (Nicastro et al., 2012).

Conclusions

The original combination of structural and functional techniques applied in this study to characterize the quadriceps muscle of

Ts65Dn mice provided a panel of data ranging from histological features to the fine organization of single muscle fiber to the muscle metabolites profile. These data highlighted hitherto unknown characteristics of the skeletal muscle in this murine model of DS. Although based on a limited number of animals, findings consistently suggest that, in the trisomic Ts65Dn mouse, the quadriceps myofibers undergo a particular form of myofiber hypertrophy associated with myofibrillar atrophy and mitochondrial alterations, which may be due to premature aging.

The present findings, while preliminary and not conclusive, constitute a solid experimental background for further investigations aimed at characterizing the biochemical and morphological underpinnings of skeletal muscle alteration in DS.

Acknowledgments. This work was supported by Departmental funding to MM and CZ.

References

Ansved T & Edström L (1991). Effects of age on fibre structure, ultrastructure and expression of desmin and spectrin in fast- and slow-twitch rat muscles. *J Anat* **174**, 61–79.

Arron JR, Winslow MM, Polleri A, Chang CP, Wu H, Gao X, Neilson JR, Chen L, Heit JJ, Kim SK, Yamasaki N, Miyakawa T, Francke U, Graef IA & Crabtree GR (2006). NFAT dysregulation by increased dosage of DSCR1 and DYRK1A on chromosome 21. *Nature* **441**, 595–600.

Baek KH, Zaslavsky A, Lynch RC, Britt C, Okada Y, Siarey RJ, Lensch MW, Park IH, Yoon SS, Minami T, Korenberg JR, Folkman J, Daley GQ, Aird WC, Galdzicki Z & Ryeom S (2009). Down's syndrome suppression of tumour growth and the role of the calcineurin inhibitor DSCR1. *Nature* **459**, 1126–1130.

Blaauw B, Canato M, Agatea L, Toniolo L, Mammucari C, Masiero E, Abraham R, Sandri M, Schiaffino S & Reggiani C (2009). Inducible activation of Akt increases skeletal muscle mass and force without satellite cell activation. *FASEB J* **23**, 3896–3905.

Bodine SC, Stitt TN, Gonzalez M, Kline WO, Stover GL, Bauerlein R, Zlotchenko E, Scrimgeour A, Lawrence JC, Glass DJ & Yancopoulos GD (2001). Akt/mTOR pathway is a crucial regulator of skeletal muscle hypertrophy and can prevent muscle atrophy in vivo. *Nat Cell Biol* **3**, 1014–1019.

Briguet A, Courdier-Fruh I, Foster M, Meier T & Magyar JP (2004). Histological parameters for the quantitative assessment of muscular dystrophy in the mdx-mouse. *Neuromuscular Disord* **14**, 675–682.

Busciglio J, Pelsman A, Wong C, Pigino G, Yuan M, Mori H & Yankner BA (2002). Altered metabolism of the amyloid beta precursor protein is associated with mitochondrial dysfunction in Down's syndrome. *Neuron* **33**, 677–688.

Canfield CA & Bradshaw PC (2019). Amino acids in the regulation of aging and aging-related diseases. *Transl Med Aging* **3**, 70–89.

Carmeli E, Ayalon M, Barchad S, Sheklow SL & Reznick AZ (2002*a*). Isokinetic leg strength of institutionalized older adults with mental retardation with and without Down's syndrome. *J Strength Cond Res* **16**, 316–320.

Carmeli E, Barchad S, Lenger R & Coleman R (2002*b*). Muscle power, locomotor performance and flexibility in aging mentally-retarded adults with and without Down's syndrome. *J Musculoskel Neuron* **2**, 457–462.

Cefalu JA, Croom WJ Jr, Eisen EJ, Jones EE, Daniel LR & Taylor IL (1998). Jejunal function and plasma amino acid concentrations in the segmental trisomic Ts65Dn mouse. *Growth Dev Aging* **62**, 47–59.

Choi JH, Berger JD, Mazzella MJ, Morales-Corraliza J, Cataldo AM, Nixon RA, Ginsberg SD, Levy E & Mathews PM (2009). Age-dependent dysregulation of brain amyloid precursor protein in the Ts65Dn Down syndrome mouse model. *J Neurochem* **110**, 1818–1827.

Cisterna B, Costanzo M, Scherini E, Zancanaro C & Malatesta M (2014). Ultrastructural features of skeletal muscle in adult and aging Ts65Dn mice, a murine model of Down syndrome. *Muscles Ligaments Tendons J* **3**, 287–294.

Consitt LA, Koves TR, Muoio DM, Nakazawa M, Newton CA & Houmard JA (2016). Plasma acylcarnitines during insulin stimulation in humans are reflective of age-related metabolic dysfunction. *Biochem Biophys Res Commun* **479**, 868–874.

Conte M, Armani A, Conte G, Serra A, Franceschi C, Mele M, Sandri M & Salvioli S (2019). Muscle-specific Perilipin2 down-regulation affects lipid metabolism and induces myofiber hypertrophy. *J Cachexia Sarcopenia Muscle* **10**, 95–110.

Costa AC, Stasko MR, Schmidt C & Davisson MT (2010). Behavioral validation of the Ts65Dn mouse model for Down syndrome of a genetic background free of the retinal degeneration mutation Pde6b(rd1). *Behav Brain Res* **206**, 52–62.

Costa AC, Walsh K & Davisson MT (1999). Motor dysfunction in a mouse model for Down syndrome. *Physiol Behav* **68**, 211–220.

Cowley PM, Keslacy S, Middleton FA, DeRuisseau LR, Fernhall B, Kanaley JA & DeRuisseau KC (2012). Functional and biochemical characterization of soleus muscle in Down syndrome mice: Insight into the muscle dysfunction seen in the human condition. *Am J Physiol Regul Integr Comp Physiol* **303**, R1251–R1260.

Cowley PM, Nair DR, DeRuisseau LR, Keslacy S, Atalay M & DeRuisseau KC (2017). Oxidant production and SOD1 protein expression in single skeletal myofibers from Down syndrome mice. *Redox Biol* **13**, 421–425.

Cowley PM, Ploutz-Snyder LL, Baynard T, Heffernan K, Jae SY, Hsu S, Lee M, Pitetti KH, Reiman MP & Fernhall B (2010). Physical fitness predicts functional tasks in individuals with down syndrome. *Med Sci Sports Exerc* **42**, 388–393.

Davisson MT, Schmidt C, Reeves RH, Irving NG, Akeson EC, Harris BS & Bronson RT (1993). Segmental trisomy as a mouse model for down syndrome. *Prog Clin Biol Res* **384**, 117–133.

Druzhyna N, Nair RG, LeDoux SP & Wilson GL (1998). Defective repair of oxidative damage in mitochondrial DNA in Down's syndrome. *Mutat Res* **409**, 81–89.

Dunn SE, Burns JL & Michel RN (1999). Calcineurin is required for skeletal muscle hypertrophy. *J Biol Chem* **274**, 21908–21912.

Ferreira DMS, Cheng AJ, Agudelo LZ, Cervenka I, Chaillou T, Correia JC, Porsmyr-Palmertz M, Izadi M, Hansson A, Martínez-Redondo V, Valente-Silva P, Pettersson-Klein AT, Estall JL, Robinson MM, Nair KS, Lanner JT & Ruas JL (2019). LIM and cysteine-rich domains 1 (LMCD1) regulates skeletal muscle hypertrophy, calcium handling, and force. *Skelet Muscle* **9**, 26.

Fukada SI (2018). The roles of muscle stem cells in muscle injury, atrophy and hypertrophy. *J Biochem* **163**, 353–358.

Gomez W, Morales R, Maracaja-Coutinho V, Parra V & Nassif M (2020). Down syndrome and Alzheimer's disease: common molecular traits beyond the amyloid precursor protein. *Aging* **12**, 1011–1033.

Gwack Y, Sharma S, Nardone J, Tanasa B, Iuga A, Srikanth S, Okamura H, Bolton D, Feske S, Hogan PG & Rao A (2006). A genome-wide *Drosophila* RNAi screen identifies DYRK family kinases as regulators of NFAT. *Nature* **441**, 646–650.

Haun CT, Vann CG, Roberts BM, Vigotsky AD, Schoenfeld BJ & Roberts MD (2019). A critical evaluation of the biological construct skeletal muscle hypertrophy: Size matters but so does the measurement. *Front Physiol* **10**, 247.

Helguera P, Seiglie J, Rodriguez J, Hanna M, Helguera G & Busciglio J (2013). Adaptive downregulation of mitochondrial function in down syndrome. *Cell Metab* **17**, 132–140.

Hendrickse P & Degens H (2019). The role of the microcirculation in muscle function and plasticity. *J Muscle Res Cell Motil* **40**, 127–140.

Johnson MA, Polgar J, Weightman D & Appleton D (1973). Data on the distribution of fibre types in thirty-six human muscles. An autopsy study. *J Neurol Sci* **18**, 111–129.

Koga S, Kano Y, Barstow TJ, Ferreira LF, Ohmae E, Sudo M & Poole DC (2012). Kinetics of muscle deoxygenation and microvascular PO(2) during contractions in rat: Comparison of optical spectroscopy and phosphorescence-quenching techniques. *J Appl Physiol (1985)* **112**, 26–32.

Koga S, Okushima D, Barstow TJ, Rossiter HB, Kondo N & Poole DC (2017). Near-infrared spectroscopy of superficial and deep rectus femoris reveals markedly different exercise response to superficial vastus lateralis. *Physiol Rep* **5**, e13402.

Landing BH & Shankle WR (1982). Reduced number of skeletal muscle fiber nuclei in Down syndrome: Speculation on a "shut off" role of chromosome 21 in control of DNA and nuclear replication rates, possibly via determination of cell surface area per nucleus. *Birth Defects Orig Artic Ser* **18**, 81–87.

Lexell J (1995). Human aging, muscle mass, and fibre type composition. *J Gerontol A Biol Sci Med Sci* **50**, 11–16.

Luther PK (2009). The vertebrate muscle Z-disc: Sarcomere anchor for structure and signaling. *J Muscle Res Cell Motil* **30**, 171–185.

Malak R, Kotwicka M, Krawczyk-Wasielewska A, Mojs E & Samborski W (2013). Motor skills, cognitive development and balance functions of children with Down syndrome. *Ann Agric Environ Med* **20**, 803–806.

Mannina L, Sobolev AP, Capitani D, Iaffaldano N, Rosato MP, Ragni P, Reale A, Sorrentino E, D'Amico I & Coppola R (2008). NMR metabolic profiling of organic and aqueous sea bass extracts: Implications in the discrimination of wild and cultured sea bass. *Talanta* **77**, 433–444.

Martins-Bach AB, Bloise AC, Vainzof M & Rahnamaye Rabbani S (2012). Metabolic profile of dystrophic mdx mouse muscles analyzed with in vitro magnetic resonance spectroscopy (MRS). *Magn Reson Imaging* **30**, 1167–1176.

Molkentin JD, Lu JR, Antos CL, Markham B, Richardson J, Robbins J, Grant SR & Olson EN (1998). A calcineurin-dependent transcriptional pathway for cardiac hypertrophy. *Cell* **93**, 215–228.

Mollo N, Cicatiello R, Aurilia M, Scognamiglio R, Genesio R, Charalambous M, Paladino S, Conti A, Nitsch L & Izzo A (2020). Targeting mitochondrial network architecture in Down syndrome and aging. *Int J Mol Sci* **21**, 3134.

Moore CS (2006). Postnatal lethality and cardiac anomalies in the Ts65Dn Down syndrome mouse model. *Mamm Genome* **17**, 1005–1012.

Nakamura E & Tanaka S (1998). Biological ages of adult men and women with Down's syndrome and its changes with aging. *Mech Ageing Dev* **105**, 89–103.

Nicastro H, da Luz CR, Chaves DF, Bechara LR, Voltarelli VA, Rogero MM & Lancha AH Jr (2012). Does branched-chain amino acids supplementation modulate skeletal muscle remodeling through inflammation modulation? Possible mechanisms of action. *J Nutr Metab* **2012**, 136937.

Nicholson JK, Lindon JC & Holmes E (1999). "Metabonomics": Understanding the metabolic responses of living systems to pathophysiological stimuli via multivariate statistical analysis of biological NMR spectroscopic data. *Xenobiotica* **29**, 1181–1189.

Nourshahi M, Damirchi A, Babaei P, Gholamali M & Salehpour M (2012). Mitochondrial biogenesis in skeletal muscle: Exercise and aging. In *Skeletal Muscle - From Myogenesis to Clinical Relations*, Cseri J (Ed.), pp. 219–242. London: IntechOpen.

Parker SE, Mai CT, Canfield MA, Rickard R, Wang Y, Meyer RE, Anderson P, Mason CA, Collins JS, Kirby RS & Correa A (2010). Updated National Birth Prevalence estimates for selected birth defects in the United States, 2004–2006. *Birth Defects Res A Clin Mol Teratol* **88**, 1008–1016.

Parra V, Altamirano F, Hernández-Fuentes CP, Tong D, Kyrychenko V, Rotter D, Pedrozo Z, Hill JA, Eisner V, Lavandero S, Schneider JW, Rothermel BA & Rothermel BA (2018). Down syndrome critical region 1 gene, rcan1, helps maintain a more fused mitochondrial network. *Circ Res* **122**, e20–e33.

Pawlikowski B, Betta ND, Elston T, Williams DA & Olwin BB (2018). Muscle stem cell dysfunction impairs muscle regeneration in a mouse model of Down syndrome. *Sci Rep* **8**, 4309.

Pereira MG, Silva MT, da Cunha FM, Moriscot AS, Aoki MS & Miyabara EH (2015). Leucine supplementation improves regeneration of skeletal muscles from old rats. *Exp Gerontol* **72**, 269–277.

Pratt SJP & Lovering RM (2014). A stepwise procedure to test contractility and susceptibility to injury for the rodent quadriceps muscle. *J Biol Methods* **1**, e8.

Recalde AL, Landing BH & Lipsey AI (1986). Increased cardiac muscle fiber size and reduced cell number in Down syndrome: Heart muscle cell number in Down syndrome. *Pediatr Pathol* **6**, 47–53.

Reeves RH, Irving NG, Moran TH, Wohn A, Kitt C, Sisodia SS, Schmidt C, Bronson RT & Davisson MT (1995). A mouse model for Down syndrome exhibits learning and behaviour deficits. *Nat Genet* **11**, 177–184.

Reinholdt LG, Ding Y, Gilbert GJ, Czechanski A, Solzak JP, Roper RJ, Johnson MT, Donahue LR, Lutz C & Davisson MT (2011). Molecular characterization of the translocation breakpoints in the Down syndrome mouse model Ts65Dn. *Mamm Genome* **22**, 685–691.

Richtsmeier JT, Baxter LL & Reeves RH (2000). Parallels of craniofacial maldevelopment in Down syndrome and Ts65Dn mice. *Dev Dyn* **217**, 137–145.

Righetti C, Peroni DG, Pietrobelli A & Zancanaro C (2003). Proton nuclear magnetic resonance analysis of meconium composition in newborns. *J Pediatr Gastroenterol Nutr* **36**, 498–501.

Rigoldi C, Galli M, Mainardi L, Crivellini M & Albertini G (2011). Postural control in children, teenagers and adults with Down syndrome. *Res Dev Disabil* **32**, 170–175.

Roth GM, Sun B, Greensite FS, Lott IT & Dietrich RB (1996). Premature aging in persons with Down syndrome: MR findings. *AJNR Am J Neuroradiol* **17**, 1283–1289.

Rothermel BA, Vega RB & Williams RS (2003). The role of modulatory calcineurin-interacting proteins in calcineurin signaling. *Trends Cardiovasc Med* **13**, 15–21.

Semsarian C, Wu MJ, Ju YK, Marciniec T, Yeoh T, Allen DG, Harvey RP & Graham RM (1999). Skeletal muscle hypertrophy is mediated by a Ca2 +-dependent calcineurin signalling pathway. *Nature* **400**, 576–581.

Shou J, Chen PJ & Xiao WH (2020). Mechanism of increased risk of insulin resistance in aging skeletal muscle. *Diabetol Metab Syndr* **12**, 14.

Sobolev AP, Mannina L, Costanzo M, Cisterna B, Malatesta M & Zancanaro C (2017). Age-related changes in skeletal muscle composition: A pilot nuclear magnetic resonance spectroscopy study in mice. *Exp Gerontol* **92**, 23–27.

Strippoli P, Petrini M, Lenzi L, Carinci P & Zannotti M (2000). The murine DSCR1-like (Down syndrome candidate region 1) gene family: Conserved synteny with the human orthologous genes. *Gene* **257**, 223–232.

Stuerenburg HJ, Stangneth B & Schoser BG (2006). Age related profiles of free amino acids in human skeletal muscle. *Neuro Endocrinol Lett* **27**, 133–136.

Tassinari V, De Gennaro V, La Sala G, Marazziti D, Bolasco G, Aguanno S, De Angelis L, Naro F & Pellegrini M (2019). Atrophy, oxidative switching and ultrastructural defects in skeletal muscle of the ataxia telangiectasia mouse model. *J Cell Sci* **132**, jcs223008.

Valenti D, de Bari L, de Rasmo D, Signorile A, Henrion-Caude A, Contestabile A & Vacca RA (2016). The polyphenols resveratrol and epigallocatechin-3-gallate restore the severe impairment of mitochondria in hippocampal progenitor cells from a Down syndrome mouse model. *Biochim Biophys Acta* **1862**, 1093–1104.

van der Meer SF, Jaspers RT, Jones DA & Degens H (2011). Time-course of changes in the myonuclear domain during denervation in young-adult and old rat gastrocnemius muscle. *Muscle Nerve* **43**, 212–222.

Yuan Y, Xu Y, Xu J, Liang B, Cai X, Zhu C, Wang L, Wang S, Zhu X, Gao P, Wang X, Zhang Y, Jiang Q & Shu G (2017). Succinate promotes skeletal muscle protein synthesis via Erk1/2 signaling pathway. *Mol Med Rep* **16**, 7361–7366.

Zancanaro C, Bolner A & Righetti C (2001). NMR spectroscopic analysis of rat brain development: In vitro proton and carbon studies of whole tissue and its phospholipid fraction. *Dev Neurosci* **23**, 107–112.

Zancanaro C, Mariotti R, Perdoni F, Nicolato E & Malatesta M (2007). Physical training is associated with changes in NMR and morphometrical parameters of the skeletal muscle in senescent mice. *Eur J Histochem* **51**, 305–310.

Zancanaro C, Nano R, Marchioro C, Sbarbati A, Boicelli A & Osculati F (1994). Magnetic resonance spectroscopy investigations of brown adipose tissue and isolated brown adipocytes. *J Lipid Res* **35**, 2191–2199.

Zancanaro C, Righetti C, Bolner A & Nano R (2002). Proton and carbon NMR spectroscopic analysis of rat liver postnatal development. *Minerva Gastroenterol Dietol* **48**, 341–345.